THEORY AND ACOUSTIC EXPERIMENTS OF NONDIFFRACTING X WAVES

J-Y. Lu and J. F. Greenleaf

Biodynamics Research Unit, Department of Physiology and Biophysics,
Mayo Clinic and Foundation, Rochester, MN 55905

ABSTRACT

Families of nondiffracting solutions of the isotropic-homogeneous wave equation have been discovered recently by the authors. These families of solutions contain some of the nondiffracting beams known previously, such as the plane wave, Durnin's nondiffracting beams, etc. One subset of the new families of nondiffracting solutions represents waves of X-like shape in a plane through the axis of the waves, which we termed "X waves." We report here the theoretical implications of one family of the nondiffracting solutions and simulate the nondiffracting X waves with finite apertures using the Rayleigh-Sommerfeld formulation of diffraction. An acoustic superposition experiment of the nondiffracting X waves in water was performed to test the theory, and the experiment agrees closely with the theory.

I. INTRODUCTION

Propagation of acoustic waves in isotropic-homogeneous media and electromagnetic waves in free space is governed by solutions of the isotropic-homogeneous (or free space) scalar wave equation. Recently, new solutions which represent beams of large depth of field have been discovered. Focused wave modes [1–2] and nondiffracting Bessel beams [3] are examples of these solutions.

We have reported the fabrication of a nondiffracting *ultrasonic annular array transducer and its applications* to medical imaging and tissue characterization [4–6]. Recently, we developed families of generalized solutions of the isotropic-homogeneous wave equation, which include Durnin's nondiffracting Bessel beams, and new nondiffracting beams, which we termed "X waves," because they have X-like shapes in a plane through the axis of the waves [7].

In this paper, we report theoretical implications of one family of the nondiffracting solutions and perform computer simulations and acoustical experiments to test the X wave theory.

One of the families of the generalized nondiffracting solutions of the isotropic-homogeneous wave equation is given by [7]

$$\Phi_\zeta(s) = \int_0^\infty T(k)\left[\frac{1}{2\pi}\int_{-\pi}^{\pi} A(\theta)f(s)d\theta\right]dk, \qquad (1)$$

where

$$s = \alpha_0(k,\zeta)r\cos(\phi-\theta) + b(k,\zeta)[z \pm c_1(k,\zeta)t], \quad (2)$$

and where

$$c_1(k,\zeta) = c\sqrt{1+[\alpha_0(k,\zeta)/b(k,\zeta)]^2}, \qquad (3)$$

where $r = \sqrt{x^2+y^2}$ represents radial coordinate, ϕ is azimuthal angle, z is axial axis, which is perpendicular to the plane defined by r and ϕ, t is time, c is speed of sound and Φ_ζ represents acoustic pressure which is a function of r, ϕ, z, and t. T(k) can be any complex function (well behaved) of k (k = ω/c is a wave number and ω is angular frequency) and could include the frequency response of an acoustic transducer. A(θ) is any complex function (well behaved) of θ and represents a weighting function of the integration with respect to θ, which is the angle around the aperture of the transducer, f(s) is any complex function (well behaved) of s, α_0(k,ζ) is any complex function of k and ζ, b(k,ζ) is any complex function of k and ζ, and k and ζ ($0 < \zeta < \pi/2$) are parameters which are independent of the spatial and time variables (r, ϕ, z, and t) of Φ_ζ(s).

If $c_1(k,\zeta)$ in Eq. (2) is real and independent of the wave number, k, then $\Phi_\zeta(s)$ in Eq. (1) represents a family of complex waves that are nondispersive, the peak of which will travel with speed, c_1, in isotropic-homogeneous media without changing wave shapes in either transverse or axial directions. This means that the waves represented by Eq. (1) are nondiffracting, i.e., both the phase and amplitude of the complex waves remain unchanged with space and time as the waves propagate. The "$\pm$" term in Eq. (2) represent the waves propagate in negative and positive z directions, respectively. In the following, we consider only waves going in positive direction (use "$-$" term).

1051-0117/91/0000-1155 $1.00

We explain the implications of Eq. (1) with the following examples:

Plane Wave

If $T(k) = \delta(k - k_0)$, where $\delta(k - k_0)$ is the Dirac-Delta function and $k_0 = \omega_0/c > 0$ is a constant, $f(s) = e^s$, $\alpha_0(k,\zeta) \equiv 0$, $b(k,\zeta) = ik$, and $A(\theta) \equiv 1$, from Eq. (1), one has the plane wave

$$\Phi_P(z) = e^{ik_0(z-ct)}. \tag{4}$$

J_0 Bessel Beam

If $T(k) = \delta(k - k_0)$, $f(s) = e^s$, $\alpha_0(k,\zeta) \equiv -i\alpha$, $b(k,\zeta) = i\beta$, and $A(\theta) \equiv 1$, from Eq. (1), we have the J_0 Bessel beam

$$\Phi_{J_0}(r,t) = J_0(\alpha r)e^{i\beta(z-c_1 t)}, \tag{5}$$

where $\beta = \sqrt{k_0^2 - \alpha^2}$ (α is a constant and $0 \le \alpha < k_0$) and $c_1 = c/\sqrt{1 - \left(\frac{\alpha}{k_o}\right)^2}$.

Zeroth-Order Broadband X Wave

We obtain the zeroth–order broadband X wave if in Eq. (1), we let $T(k) = a_0 e^{-a_0 k}$, $f(s) = e^s$, $\alpha_0(k,\zeta) = -ik\sin\zeta$, $b(k,\zeta) = ik\cos\zeta$, and $A(\theta) \equiv 1$:

$$\Phi_{XBB_0} = \frac{a_0}{\sqrt{(r\sin\zeta)^2 + [a_0 - i\cos\zeta(z - c_1 t)]^2}}, \tag{6}$$

where $c_1 = c/\cos\zeta$, $a_0 > 0$ is a constant, and ζ is the angle between the propagation direction of the plane waves that compose the X waves and the axial axis, z.

Figure 1 shows the exact nondiffracting beams represented by Eqs. (4)-(6). These beams are assumed to be produced with an infinite aperture and infinite energy, and will propagate to infinite distance without changing their complex waveforms. For comparison, Fig. 2 shows some typical diffracting beams (Gaussian beam and focused beam). These beams remain diffracting even if they are produced with an infinite aperture and infinite energy. However, the exact nondiffracting beams are not physically realizable because they require an infinite aperture and infinite energy, and may not be causal. But, real beams can closely approximate theoretical beams depending on the aperture size and energy. Figure 3 shows finite aperture approximations of the nondiffracting beams in Fig. 1. Of course, finite aperture produces finite depth of nondiffraction (finite depth of field, Z_{max}). Because the approximated nondiffracting beams have large depth of field as compared to the conventional focused beams, they could have practical importance and could be applied to various wave related fields. The depth of fields of the finite aperture approximations of the nondiffracting beams (see Fig. 3) are given by

$$Z_{max} \approx \frac{\pi a^2}{\lambda} \text{ (plane wave)}, \tag{7}$$

$$Z_{max} \approx a\sqrt{(k/\alpha)^2 - 1} \text{ (Bessel beams)}, \tag{8}$$

$$Z_{max} \approx a\cot\zeta \text{ (X waves)}, \tag{9}$$

where a is the radius of the aperture and λ is the wavelength.

In the following, we report the simulations and experimental productions of the newly discovered "X waves."

II. SIMULATIONS, EXPERIMENTS AND RESULTS

A zeroth–order X wave is simulated with the Rayleigh–Sommerfeld formulation of diffraction [8]. The transducer is assumed to have a 50 mm diameter. The transfer function of the transducer is assumed to be a Blackman window function [9] with its peak on 2.5 MHz and −6 dB bandwidth around 2.1 MHz. The time dependent aperture weighting function used in the Rayleigh–Sommerfeld formula is calculated from Eq. (6) by setting z = 0. The parameters ζ (which is θ in Fig. 4) and a_0 are 4° and 0.05 mm, respectively.

The simulated zeroth–order X waves at distances z = 170 mm and 340 mm are shown in Panels (1) and (2) of Fig. 4, respectively. The X waves are axially symmetric (the axis is in left-right direction and through the wave peak). The panel size is 10 mm (width) × 25 mm (height). The brightness of pixels in Fig. 4 represents the pressure envelope of the X waves.

Panels (3) and (4) are experimental results corresponding to the simulations in Panels (1) and (2), respectively. A 50–mm diameter annular array ultrasonic transducer was used for the experiment. The transducer has 10 elements, a central frequency of 2.5 MHz, and is the same one that we used to produce the J_0 Bessel nondiffracting beam [3–6]. The −6 dB pulse–echo (two way) bandwidth of the transducer is around 50% of its central frequency. The transducer is made with PZT ceramic/polymer composite and its impedance is matched to that of water. The drive function for each transducer element was calculated from Eq. (6) by setting z = 0 and setting r to the average diameter of that element (quantized in 10 segments) and truncated at $\pm 5\mu s$ in time.

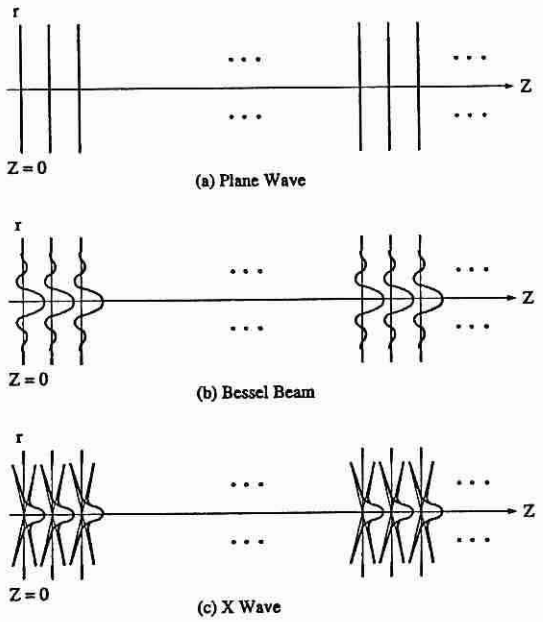

Fig. 1 Examples of exact (theoretical) nondiffracting beams which are symmetric around the z axis and produced by an infinite aperture and infinite energy. (a) Plane wave (b) J_0 Bessel beam (c) Zeroth–order broadband X wave.

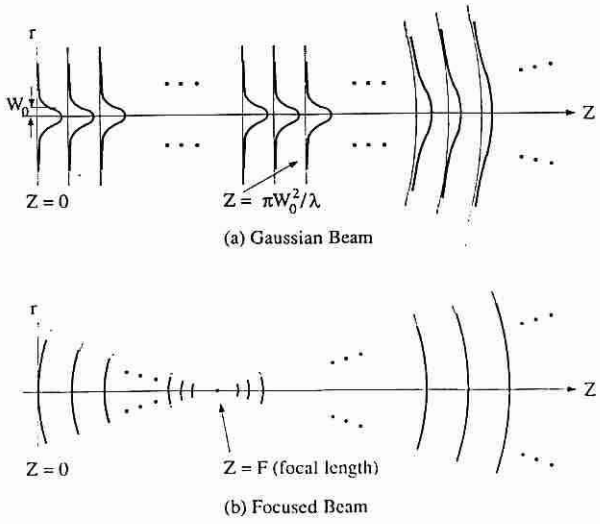

Fig. 2 Examples of diffracting beams which are symmetric around the z axis and produced by an infinite aperture and infinite energy. (a) Gaussian beam with FWHM (full width at half maximum) of $2W_0$ (b) Focused spherical wave with focal length of F.

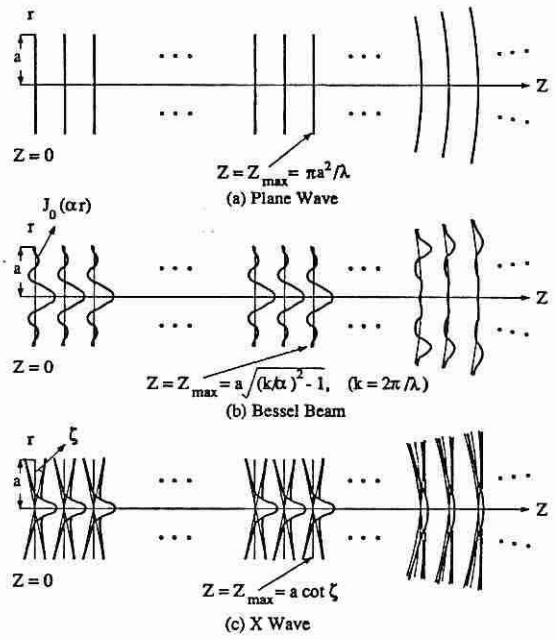

Fig. 3 Finite aperture approximations of the exact nondiffracting beams shown in Fig. 1. In addition to the well-known plane wave, these approximated beams are very close to the exact ones within their finite aperture sizes and depth of fields. Beyond the depth of fields, they diffract. (a) Finite aperture plane wave (b) Finite aperture J_0 Bessel beam (c) Finite aperture zeroth–order broadband X wave.

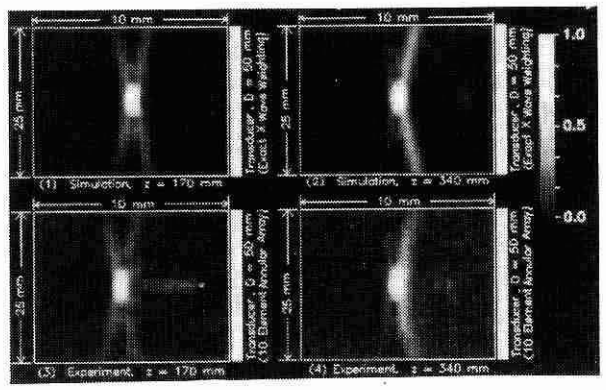

Fig. 4 Panels (1) and (2): Computer simulations of the zeroth-order band-limited nondiffracting X wave at distances z = 170 mm and 340 mm, respectively, away from the surface of a 50 mm diameter transducer. Exact X wave aperture shading and broadband X wave pulse drive of the transducer were assumed. The transmitting transfer function of the transducer was assumed to be the Blackman window function peaked at 2.5 MHz and with −6 dB

dB bandwidth around 2.1 MHz. Panels (3) and (4): Experimental results which correspond to the simulations in (1) and (2), respectively. A 10 element, 50 mm diameter, 2.5 MHz central frequency, PZT ceramic/polymer composite J_0 Bessel nondiffracting transducer [4,5] with a -6 dB pulse-echo bandwidth about 50% of the central frequency was used. The panel size is 25 mm (height) x 10 mm (width), and the parameters a_0 and ζ are 0.05 mm and 4°, respectively. Linear analytic envelope of the real part of the X waves is displayed in all panels. [Reproduced with permission from J-y. Lu and J. F. Greenleaf, "Experimental verification of nondiffracting waves," IEEE Transactions on Ultrasonics, Ferroelectrics, and Frequency Control]

In the experiments, a Polynomial Waveform Generator (Model Data 2045) was used to produce the drive signals. The signals were amplified to excite the transducer element by element. The acoustic fields were measured by a 0.5 mm diameter calibrated hydrophone and superposed over the 10 transducer elements to produce the X waves.

It is seen from Fig. 4 that the experiments agree closely with the simulations. The X waves are peaked on the wave centers and keep in focus at all distances (here we show examples at z = 170 mm and 340 mm) within its depth of field. It is obvious that the depth of field of the experimental X waves is larger than 340 mm which is predicted by the theory (about 358 mm—calculated from Eq. (9)).

The -6 dB lateral and axial beamwidths of the experimental X waves measured from Fig. 4 through the wave peaks are 4.7 mm and 0.65 mm, respectively. With the same -6 dB lateral beamwidth and central frequency of the X waves, an unfocused Gaussian beam will have only about 28.9 mm depth of field (Rayleigh distance) in water.

III. DISCUSSION

Sidelobes

Although the X waves have large depth of field, their sidelobe (X branch) level is higher than that of the conventional focused beams, which will reduce the image contrast when the X waves are applied to medical imaging. Figs. 5(1) and 5(2) show the beam plots along highest X branches through the peak of the X waves at distances z = 170 mm and 340 mm, respectively.

Figure 5 shows that the experiments are very close to the simulations. The sidelobes of the X waves are higher at z = 340 mm. One possible way to reduce the effects of the sidelobes in imaging systems is to use X waves to transmit and the conventional dynamically focused beams to receive, which would combine the advantage of the large depth of field of the X waves with the advantage of low sidelobes of the conventional focused beams.

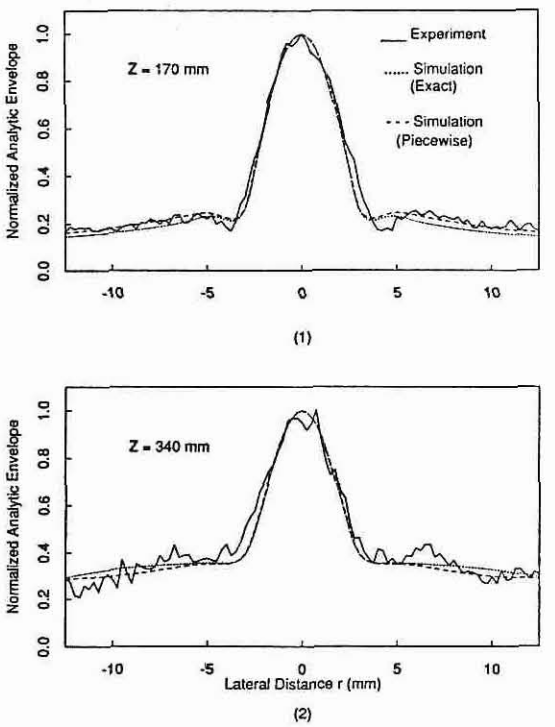

Fig. 5 Beam plots along the highest X branches of the X waves in Fig. 1 at distances (1) z = 170 mm and (2) 340 mm. Full lines, dotted lines, and dashed lines correspond to experiments, simulations with an exact X wave aperture shading and simulations with a 10–segment piecewise annular X wave aperture shading (corresponding to the element geometry of the transducer used in the experiments), respectively.

Total Energy and Energy Density

From Eq. (6), it is seen that the total energy of X waves is infinite, but the energy density is finite everywhere at any time. The finite energy density makes it possible to closely approximate the theoretical X waves with practical waves.

Causality

Equation (6) shows that the theoretical X waves are noncausal. But the theoretical X waves can be approximated by truncating their infinite time duration to a short value, $\pm 5\mu s$ in our experiment, relative to the center of the waves. This value must increase as the aperture increases to ensure a good approximation of the X waves.

Speed of X Waves

The theoretical X waves (see Eq. (6)) are superluminal, i.e., the speed of the X wave peak is greater than the speed of sound in the acoustical case and the speed of light in the optical case. But the approximated X waves result from the interference of causal waveforms in a finite aperture and each of the wavelets causing the interference travels at the speed of sound or light. More discussions on the speed of X waves are contained in Reference [7].

Parameters a_0 and ζ

The parameter a_0 determines the fall-off speed of the high frequency components of the X waves (see Eq. (6)). Bigger a_0 results in a faster fall-off of the high frequency components and is associated with larger lateral and axial beamwidths of the X waves [7].

ζ is the angle of the propagation direction of the plane waves that compose the X waves relative to the z axis. The zeroth–order broadband X wave is a superposition of plane waves, all having the same amplitude and traveling at a fixed angle, ζ, with their azimuthal angle, θ, ranging from 0 to 2π over a large frequency range. Bigger ζ will produce X waves of larger lateral resolution but bigger axial beamwidth and reduced depth of field (see Eq. (9)) [7].

IV. CONCLUSION

One subset of the families of nondiffracting solutions to the isotropic-homogeneous scalar wave equation which we termed "X waves" can be approximated closely with finite aperture and causal drive signals. The physically produced X waves have large depth of field and are nondiffracting over a finite distance. The large depth of field of the X waves make them potentially useful in medical imaging, tissue characterization, and nondestructive evaluation of materials. The effects of high sidelobes (X branches) of X waves in imaging could be reduced by using the X waves to transmit and conventional dynamically focused beams to receive.

V. ACKNOWLEDGMENTS

The authors appreciate the help of Thomas M. Kinter in developing software for data acquisitions. The authors also appreciate the help of Randall R. Kinnick in making transformers to drive the transducer. The authors appreciate the secretarial assistance of Elaine C. Quarve and the graphic assistance of Christine A. Welch. This work was supported in part by grants CA 43920 and CA54212–01 from the National Institutes of Health.

VI. REFERENCES

1. J. B. Brittingham, "Focus wave modes in homogeneous Maxwell's equations: transverse electric mode," J. Appl. Phys., vol 54, no. 3, pp. 1179–1189, 1983.
2. R. W. Ziolkowski, D. K. Lewis, and B. D. Cook, "Evidence of localized wave transmission," Phys. Rev. Lett., vol. 62, no. 2, pp. 147–150, Jan. 9, 1989.
3. J. Durnin, J. J. Miceli, Jr., and J. H. Eberly, "Diffraction-free beams," Phys. Rev. Lett., vol. 58, no. 15, pp. 1499–1501, April 13, 1987.
4. Jian-yu Lu and J. F. Greenleaf, "Ultrasonic nondiffracting transducer for medical imaging," IEEE Trans. UFFC, vol. 37, no. 5, pp. 438–447, Sept., 1990.
5. Jian-yu Lu and J. F. Greenleaf, "Pulse-echo imaging using a nondiffracting beam transducer," US Med. Biol., vol. 17, no. 3, pp. 265–281, May, 1991.
6. Jian-yu Lu and J. F. Greenleaf, "Evaluation of a nondiffracting transducer for tissue characterization," 1990 Ultrasonics Symposium Proceedings, Honolulu, HI, 90CH2938–9, vol. 2, pp. 795–798, Dec. 4–7, 1990.
7. Jian-yu Lu, and J. F. Greenleaf, "Nondiffracting X waves—exact solutions to free-space scalar wave equation and their finite aperture realizations," IEEE Trans. UFFC (to be published in Vol. 39, No. 1, Jan., 1992).
8. J. W. Goodman, *Introduction to Fourier Optics*. New York, NY: McGraw-Hill, 1968, chs. 2–4.
9. A. V. Oppenheim and R. W. Schafer, *Digital Signal processing*. Englewood Cliffs, NJ: Prentice-Hall, Inc., 1975, ch. 5.